Available online at www.sciencedirect.com

SCIENCE DIRECT®

Journal of Volcanology and Geothermal Research 137 (2004) 231–246

Journal of volcanology and geothermal research

www.elsevier.com/locate/jvolgeores

Pulsed lava effusion at Mount Etna during 2001

Nicole C. Lautze[a,*], Andrew J.L. Harris[a,b], John E. Bailey[a,b], Maurizio Ripepe[c], Sonia Calvari[d], Jonathan Dehn[e], Scott K. Rowland[b], Kate Evans-Jones[f]

[a] *Department of Geology and Geophysics, SOEST, University of Hawaii, 1680 East–West Road, Post 606A, Honolulu, HI 96822, USA*
[b] *HIGP/SOEST, University of Hawaii, Honolulu, HI 96822, USA*
[c] *Dipartimento di Scienze della Terra, Università di Firenze, Florence, Italy*
[d] *Istituto Nazionale di Geofisica e Vulcanologia-Sezione di Catania, Catania, Italy*
[e] *Alaska Volcano Observatory, Fairbanks, AK, USA*
[f] *NERC Remote Sensing Data Analysis Service, Plymouth Marine Laboratory, Plymouth, UK*

Abstract

Effusion rate and degassing data collected at Mt. Etna volcano (Italy) in 2001 show variations occurring on time scales of hours to months. We use both long- and short-term data sets spanning January to August to identify this variation. The long data sets comprise a satellite- and ground-based time series of effusion rates, and the latter include field-based effusion rate and degassing data collected May 29–31.

The satellite-derived effusion rates for January through August reveal four volumetric pulses that are characterized by increasing mean effusion rate values and lead up to the 2001 flank eruption. Peak effusion rates during these 23–57 day pulses were 1.2 $m^3\ s^{-1}$ in Pulse 1 (1 Jan–4 Mar), 1.1 $m^3\ s^{-1}$ in Pulse 2 (5 Mar–21 Apr), 4.2 $m^3\ s^{-1}$ in Pulse 3 (24 Apr–18 Jun), 8.8 $m^3\ s^{-1}$ in Pulse 4 (23 Jun–16 Jul), and 22.2 $m^3\ s^{-1}$ during the flank eruption (17 Jul–9 Aug). Rank-order analysis of the satellite data shows that effusion rate values during the 2001 flank eruption define a statistically different trend than Etna's persistent activity from Jan 1 to Jul 17. Data prior to the flank eruption obey a power-law relationship that may define an effusion rate threshold of $\sim 3–5\ m^3\ s^{-1}$ for Etna's typical persistent activity.

Our short-term data coincide with the satellite-derived peak effusion period of Pulse 3. Degassing (at-vent puff frequency) shows a general increase from May 29 to 31, with hour-long variations in both puff frequency and lava flow velocity (effusion rate). We identify five 3–14 h degassing periods that contain 26 shorter (19–126 min-long) oscillations. This variation shows some positive correlation with effusion rate measurements during the same time period. If a relationship between puff frequency and effusion rate is valid, we propose that their short-term variation is the result of changes in the supply rate of magma to the near-vent conduit system. Therefore, these short-term data provide some evidence that the clear weeks- to months-long variation in Etna's effusive activity (January–August 2001) was overprinted by a minutes- to hour-scale oscillation in shallow supply.

Keywords: effusion rate; degassing; oscillation; shallow supply; Etna

1. Introduction

That mass flux rates can vary over time scales of days to months during episodic, effusive basaltic eruptions is well known. Wadge (1981) showed that

* Corresponding author. Tel.: +1-808-956-5960; fax: +1-808-956-5512.
E-mail address: nlautze@soest.hawaii.edu (N.C. Lautze).

0377-0273/$ - see front matter © 2004 Elsevier B.V. All rights reserved.
doi:10.1016/j.jvolgeores.2004.05.018

on such time scales, mass fluxes during a basaltic eruption often reach a maximum value after a short period of waxing flow. The release of elastic strain then causes the mass eruption rate to fall more slowly than it rose. However, during persistent basaltic eruptions, magma supply and mass flux rates are generally assumed to be broadly constant. Allard et al. (1994) estimated that persistent degassing and mild explosive and effusive activity at Stromboli (Italy) has been maintained by a mass flux of 0.01–0.02 km^3 $year^{-1}$ for over ~ 2000 years. Harris et al. (2000) identified a similar, generally steady effusion rate characterizing persistent summit activity at Mount Etna (Italy) from 1980 to 1995. There is mounting evidence, however, that this activity shows considerable short-term variation (Tilling et al., 1987; Swanson et al., 1979).

Recent experiments on Stromboli volcano (Italy) indicate that mass flux to persistently active basaltic systems may proceed in a pulsatory manner. At Stromboli, Ripepe et al. (2002) recorded positively correlated variations in degassing and explosive activity, with 5–40 min phases characterized by either vigorous or weak degassing. Ripepe et al. (2002) suggest that this is consistent with variations in the rate at which the shallow system is supplied by gas-rich magma. At Erta Ale (Ethiopia), however, cyclic variations in the surface activity of a basaltic lava lake (~ 1–2 h) can be accommodated within a model in which supply is constant, and surface variation is caused by convective instabilities within the lake itself (Harris et al., 1999).

An ideal way to identify variations in mass flux at persistently active volcanic systems is to make detailed effusion rate measurements over hours to months. Here, we achieve this through an examination of the persistent effusive activity at Etna that preceded the flank eruption during July–August 2001. In an effort to characterize the time-varying nature of persistent basaltic activity, this paper presents: (1) a satellite- and ground-based effusion rate time series at Etna from January through August 2001; and (2) effusion rate and degassing data collected at Etna during a field experiment May 29–31, 2001.

2. Etna's activity during 2001

This section presents a qualitative description of Etna's activity in 2001. It is intended as a narrative leading into the quantitative description of pulsatory effusive activity that ensues. We note that this description includes explosive activity, which is not incorporated in the later data.

The current structure of Etna volcano consists of four summit craters and a fissure system that trends northeast and south (Fig. 1). Persistent activity from January to July 17 was concentrated at Southeast Crater (SEC). Through April, activity was primarily effusive and characterized by low, but generally increasing, effusion rates of 1–3 m^3 s^{-1}. Strombolian activity commenced during the first half of May and was accompanied by heightened effusion rates (up to a maximum of 12 m^3 s^{-1}), which persisted through the second half of June. Episodic fire fountaining events in May, June, and July were followed by a flank eruption during July 17–August 9. This was followed by a hiatus in activity that lasted until March 2002. We review the activity in more detail below.

2.1. Last months of 2000–April 2001

Activity at Etna during late 2000 and the initial months of 2001 consisted of episodic Strombolian and ash explosions from Bocca Nuova (BN) and SEC and lava emission from the N flank of SEC. BN exhibited intermittent, low-intensity emission of gas and lithic ash at a consistently increasing frequency through January. Strombolian activity, juvenile ash emissions, and strong degassing occurred at BN throughout February, increasing slightly through March and April.

Strombolian activity at SEC commenced on January 15, peaked 3 days later, and stopped by January 21. Lava emission from a fissure at an elevation of 3080 m on the N flank of SEC began January 21 and proceeded discontinuously through late April. Effusive activity from additional vents at 3100 and 3150 m on the N flank of SEC commenced during early February. The 3100-m flow continued for several days, and the 3150-m flow persisted until the end of February. Effusive activity escalated during March and April, with an increase in effusion rate at the 3080-m vent, and the opening of an effusive vent on SEC's east flank on April 8 (Andronico et al., in preparation). Still, effusion rate throughout the period was generally less than 1 m^3 s^{-1} and increased to 2–3 m^3 s^{-1} only on April 27 (Andronico et al., in preparation). Degassing at SEC was observed to increase during the last days of April.

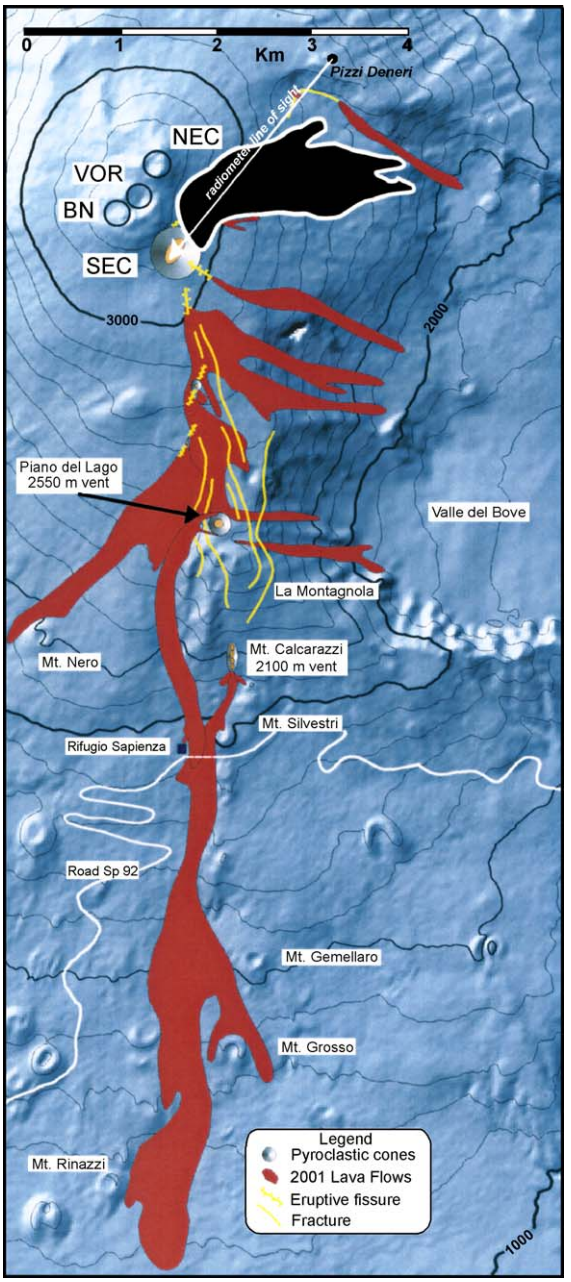

Fig. 1. Map of Etna showing the location of the main volcanic centers and flows (in gray) associated with the 2001 flank eruption. Also, note the approximate location of the flow field active during our field experiment May 29–31 to NE of SEC (black with white outline; identified using a Landsat ETM+ image for July 13, 2001) and the location of Pizzi Deneri with the line of sight from the puff monitoring IR-thermometer to the SEC as indicated (figure modified from EOS article by Calvari et al., 2001).

2.2. May–July 17, 2001

Between May and mid-July, variable but heightened effusive activity at SEC was accompanied by an increase in the frequency of explosive events and the onset of fire fountain episodes. Activity at BN was inconsequential.

In the first days of May, weak spattering from the north fissure of SEC formed hornitos around the vents, and amplified effusion rates peaked at 10–12 $m^3\ s^{-1}$ on May 3 (Andronico et al., in preparation). Strombolian activity from the summit of SEC (not witnessed since January 21) resumed on May 7, and the first fire fountain event of the year occurred May 9. A vent at 3150 m opened with an effusion rate of 2.5–4.5 $m^3\ s^{-1}$ on May 18 (Andronico et al., in preparation). Heightened activity during the final days of May was marked by the occurrence of Strombolian activity also at Northeast Crater (NEC), a sharp increase in Strombolian activity at SEC on May 28, and effusion rates from the N base of SEC increasing to 6–8 $m^3\ s^{-1}$ during May 29–30 (Andronico et al., in preparation).

Fourteen paroxysmal episodes occurred between June 1 and July 17, mostly from a vent on the N flank of SEC. During such events, continuous fire fountaining persisted for up to 1 h and was accompanied by degassing at all of the summit craters and lava effusion from SEC's N flank fissure. The fire fountaining generally fed short-lived (hour to day) lava flows. The episodes were preceded by a 5–11 h increase in Strombolian and effusive activity.

On July 13, the final paroxysm of this period occurred with a seismic swarm and the opening of fissures along SEC's S flank.

2.3. 2001 flank eruption (July 17–August 9)

A flank eruption began at 07:00 (local time) on July 17, at a fissure at 2950 m extending south from the base of the SEC. Vents farther to the south at 2700 and 2100 m opened during July 17–18, and a fourth vent was established at 2550 m during July 19. Minor vents opened to the northeast of the SEC during July 20–23, but by July 19 and for the majority of the eruption, activity had become concentrated along a ~ 7-km-long, ~ N–S-trending field of fissures on the south flank (Fig. 1). The dominant effusive centers at 2700 and 2100 m were consistently active through-

out the eruption. Flows from the 2100-m fissure extended ~ 3.5 km southward to the 1350-m contour by July 19, causing authorities to declare a state of emergency. This vent ultimately produced the longest (6.5 km) and volumetrically largest ($18–24 \times 10^6$ m^3 bulk) lava flow of the eruption. On July 22, fast moving flows from the 2700-m fissure destroyed several ski lifts and approached the tourist complex at the Refugio Sapienza. Flows from 2950 and 2550 m were shorter, extending a maximum distance of 2–3 km by the end of July.

Major explosive activity was focused at the 2550-m vent. Phreatomagmatic eruptions produced thick ash clouds from its opening on July 19 through July 24. Between July 24 and 25, there was a shift to fire fountaining activity, which rapidly formed the main cone of the eruption. In the last days of July, there was a return to ash-dominant emission. The effusion rate at the 2100-m fissure began to decline ~ August 1 and was followed by a similar decrease at the 2900- and 2700-m vents within the following days. Activity at 2550 m ceased August 6, and the last emission of lava was observed at the 2100-m vent August 9.

The 24-day-long flank eruption emplaced an ~ 4.7-km^2 lava flow field on Etna's south flank (Fig. 1), with a preliminary estimated bulk volume of 48×10^6 m^3 and a time-averaged lava effusion rate of 24 m^3 s^{-1} (Calvari et al., 2001). Corrected for a vesicularity of $22 \pm 12\%$ (after Harris et al., 2000), this gives a DRE volume of $32–43 \times 10^6$ m^3 for effusive activity and a mean lava effusion rate of 15–21 m^3 s^{-1}.

2.4. Post-2001 flank eruption

The months following the 2001 flank eruption through March 2002 were strikingly quiet and marked the longest noneruptive interval at Etna since 1995. No fresh magma appeared in the summit craters, and activity was typified solely by fumarolic activity and occasional collapse at the four summit craters.

Between March and September 2002, sporadic Strombolian activity resumed at NEC and BN. Etna then returned to a state of calm from September 22 through October 26. A seismic swarm that began late in the evening of October 26, 2002 forewarned the onset of a new flank eruption on October 27. This eruption continued until January 28, 2003. It exhibited a number of phases distinguished by variations in eruption style and involved activity at both Etna's south and northeast fissure systems.

3. Data and methods

Our data set consists of: (1) lava effusion rate values for January–August 2001 that are derived from satellite- and ground-based methods; and (2) effusion rate and degassing data obtained during a field experiment May 29–31, 2001. We use the latter data to track variation on time scales of minutes to days and as a check on day- to month-long trends apparent in the longer time series.

3.1. Long-term effusion rates, January–August 2001

3.1.1. Satellite-based methods

Thermal data from the advanced very high resolution radiometer (AVHRR) flown aboard NOAA satellite series were used to obtain DRE effusion rate estimates following methodologies given in Harris et al. (1997a,b, 2000). AVHRR provides up to four images per day of Etna, though images with cloud cover are unusable (Harris et al., 1997b). Thermal data were received at the University of Dundee and processed in real time at the Plymouth Marine Laboratory (U.K.). Calibrated data were transferred from Plymouth to the Hawaii Institute of Geophysics and Planetology, where hotspot products were posted on the Web (http://hotspot.higp.hawaii.edu/etna/ and http://goes.higp.hawaii.edu/cgi-bin/imageview). During the 2001 flank eruption, this system enabled scientists at the Istituto Nazionale di Geofisica e Vulcanologia-Sezione di Catania (INGV-CT) to view AVHRR-derived effusion rate values within 6 h of data reception. Together with ground-based measurements collected by INGV-CT, these data were used during the eruption for hazard assessment and civil protection purposes.

For this study, all AVHRR images obtained for the period January 1–August 9, 2001 were manually scrutinized for image quality, cloud cover, and the presence or absence of a thermal anomaly in Etna's summit region. A total of 207 cloud-free images with anomalous thermal radiance due to volcanic activity were identified.

Effusion rate values for each image were obtained by summing estimates of the radiative, convective, and conductive heat loss for each anomalous pixel. Calculation of these heat losses requires the area (A_{lava}) and surface temperature (T_{lava}) of the lava in each pixel (Harris et al., 1997a,b, 2000). When possible, these values were attained using the dual-band method of Dozier (1981) and Rothery et al. (1988). The dual-band method yields the fraction of a pixel occupied by hot lava (p) and the lava surface temperature (T_{lava}) by using two bands of AVHRR thermal data (R_3 and R_4) that are each corrected for surface emissivity, atmospheric transmissivity, upwelling, and solar reflection, and the following equations:

$$R_3 = pL_3(T_{lava}) + (1-p)L_3(T_b) \quad (1a)$$

$$R_4 = pL_4(T_{lava}) + (1-p)L_4(T_b) \quad (1b)$$

L_x is the Planck function for a blackbody at wavelength x and temperature T, and T_b is the approximate pixel background temperature. The value of T_b was obtained from the nearest, non-anomalous pixel. Eqs. (1a) and (1b) can then be solved for p and T_{lava}. Multiplying p by the AVHRR pixel area of 10^6 m^2 yields A_{lava}.

In some cases, AVHRR band 3 (R_3) was saturated, and therefore the single-band method described in Harris et al. (1997a,b) was used. In this method, assuming a range for T_{lava} allows p to be calculated from Eq. (1b). Effusion rate (ER) is now calculated as a function of lava area according to the equation $ER = xA_{lava}$ (in which x is a thermally defined constant) (Wright et al., 2001).

AVHRR band 3 saturation occurs at a pixel-integrated temperature of ~ 50 °C (Harris et al., 1995). Assuming a lava surface temperature of 500–1000 °C against a background of 0–25 °C, R_3 will reach saturation when the lava area reaches 10^2–10^3 m^2 ($p = 10^{-3}$–10^{-4}). AVHRR band 4, on the other hand, will not saturate until the lava area reaches $1–4 \times 10^4$ m^2 ($p = 10^{-2}$–4×10^{-2}). No pixels saturated in band 3 were observed during January through April, which is consistent with the low level of effusive activity during this time. From May 1 through August 9, however, band 3 was saturated in all cloud-free images and thus the single-band method was applied. The effusion rate values calculated from AVHRR images are presented as 'satellite-derived' in Fig. 2.

3.1.2. Ground-based methods

Ground-based estimates were made in one of two ways. Prior to the 2001 flank eruption, values were obtained following the methodology of Calvari et al. (2003). This approach uses measurements of a lava channel width (w), depth (d), and maximum velocity of flow in the channel (V_{max}) (and assumes a semicircular channel geometry) to obtain instantaneous bulk volume effusion rates (ER) from $ER = 0.67V_{max}wd$. During the 2001 flank eruption, values were obtained using the method given in Calvari et al. (1994), wherein the area (A) and thickness (d) of flow units emplaced during a known period of time (t) are used to calculate bulk mean effusion rates (ER) from $ER = Ad/t$. We corrected all values for vesicularity of 22 ± 12% to convert from bulk to DRE values (Harris et al., 2000). These data are presented as 'ground-based' in Fig. 2.

3.2. Short-term effusion rates and degassing, May 29–31, 2001

3.2.1. Effusion rate calculations from channel-fed activity

Lava effusion from a vent on the NE flank of SEC fed a compound flow field throughout the duration of our field experiment (see Fig. 1 for approximate location). A well-established master channel ~ 1.5 m deep and ~ 3 m wide fed multiple ′a′ a flows that extended no more than 2 km from the vent and contributed to an ~ 1-km-wide flow field extending northwards from the SEC. Flow in the channel was not stable, with 10–30 min surges in effusion breaking 1–3 h periods of steady-to-waning flow. During each surge, an increase in effusion rate developed over some minutes, causing channel overfill and the formation of short-lived flow units that extended a few tens of meters.

To track changes in the flow velocity in the master channel, a forward looking infrared (FLIR) thermal imager was aimed onto the channel surface ~ 250 m down-flow from the vent. The FLIR collected images at a rate of 1 image every 10 s from approximately 14:45 to 18:30 on May 30 and 12:00 to 13:45 and 15:00 to 17:00 on May 31. We obtained flow velocities by tracking the transit of pieces of crust in at least three consecutive images. Given these channel dimensions and measured flow velocities, bulk effusion rate

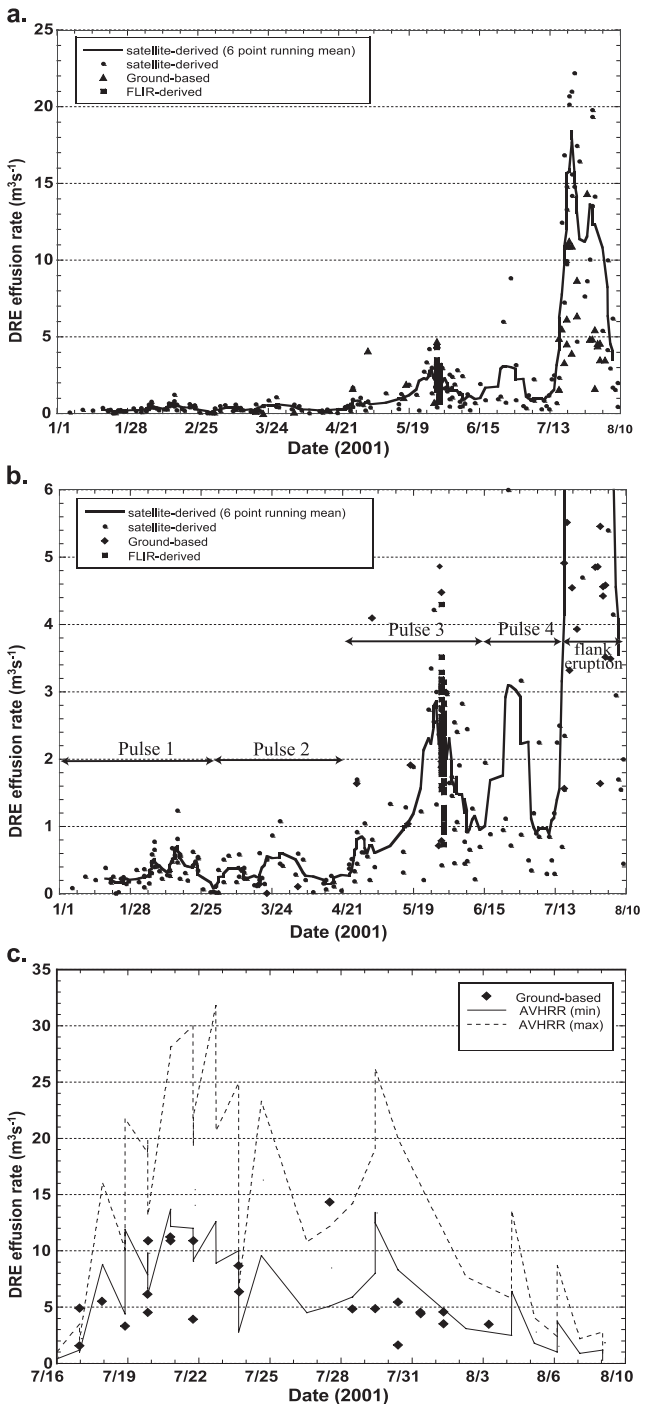

Fig. 2. Complete effusion rate database, including satellite-derived, ground-based, and FLIR-derived data: (a) entire range of effusion rate values for January 1–August 9, 2001; (b) detail of the effusion rate range from 0 to 6 $m^3 s^{-1}$ for January 1–August 9, 2001 with arrows indicating the four identified effusion rate pulses preceding the 2001 flank eruption; (c) detail of the 2001 flank eruption.

values were calculated following the method of Calvari et al. (2003), and DRE values were attained by correcting for a vesicularity of 22%. These data are presented as 'FLIR-derived' in Fig. 2.

3.2.2. Degassing from SEC, May 29–31, 2001

During our field experiment, persistent degassing from the summit of SEC occurred as a discrete burst, or puff, every few seconds (Fig. 3). The model of Ripepe et al. (2002) explains puffs as caused by the ascent of bubble bands in the conduit. Each band generates a pulse in gas emission, or puff, upon reaching the free lava surface in the conduit. Ripepe et al. (in press) infer that periods of rapid degassing are associated with a high puff frequency (high frequency of bubble band rise), and periods of low degassing are associated with a low puff frequency.

Following the approach of Ripepe et al. (2002), we pointed an Omega OS 554, 8–14 μm, thermal infrared (IR) thermometer at the SEC summit to monitor the frequency and relative temperature (amplitude) of the puffing. The radiometer was placed at Pizzi Deneri, a distance of ~ 2.5 km from the SEC summit (Fig. 1), and targeted using the thermal signal of puffs (i.e. the summit was scanned until a good, oscillating signal was obtained). Given this distance and the 1° field of the sensor, the recorded thermal radiance covered an ~ 45-m circular field of view (FOV) that was centered on the plume, but included portions of the cone and sky (Fig. 3). Excellent visibility and low wind speed

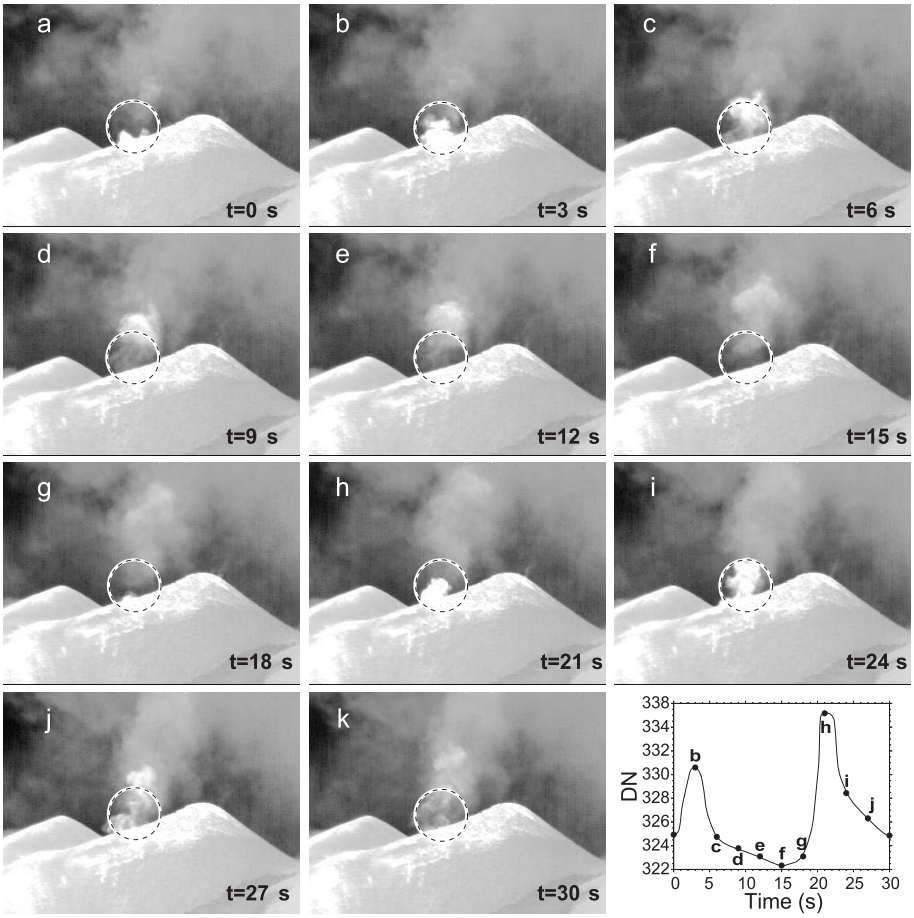

Fig. 3. Time series of FLIR thermal images that shows two gas puffs rising from SEC. The dashed circle represents the approximate field of view of the thermal infrared radiometer. The inset graph shows a schematic time series of IR-thermometer data (DN = digital number). Letters in individual images correspond to points shown on inset.

throughout our data collection period were made for optimal observation conditions.

With the integrated thermal radiance converted to temperature, gas puffs are expressed as oscillations in the temperature record (Fig. 4). Data were collected continuously at an 18×10^{-3} s sampling interval beginning at 21:10 on May 29 and ending at 16:40 on May 31, except during an ~3-h power failure during the morning of May 30. Three sample data sets showing variation in puff frequency and apparent amplitude are shown in Fig. 4.

The thermal signal of puffs may show a diurnal variation (Fig. 5). If so, it can be explained by variation in the temperature of the volcanic edifice, combined with the relatively low temperature of the gas plume. Ground surface temperatures ranged from below freezing at night to 60 °C during the day. A reasonable FOV comprised 40% cone at either 0 or 60 °C and 60% sky at −18 °C will yield approximate FOV integrated temperatures of −10 and 21 °C, respectively. A FOV with 10% gas (puff) at 75 °C, 40% cone at either 0 or 60 °C, and 50% sky at −18 °C will yield FOV integrated temperatures of 3 and 31 °C, respectively. Thus, the magnitude of the same puff appears as 13 °C when the cone is relatively cold (i.e. during nighttime hours) and 10 °C when the cone is relatively warm. Fig. 5 shows a time series of apparent puff amplitude (measured as the maximum per-minute relative FOV integrated temperature change or maximum per-minute amplitude of a spike as shown in Fig. 4). Note that puffs appear to be higher amplitude during the nighttime hours from May 30 to 31 and decrease during the daylight hours on May 31. Though our data lend evidence that a

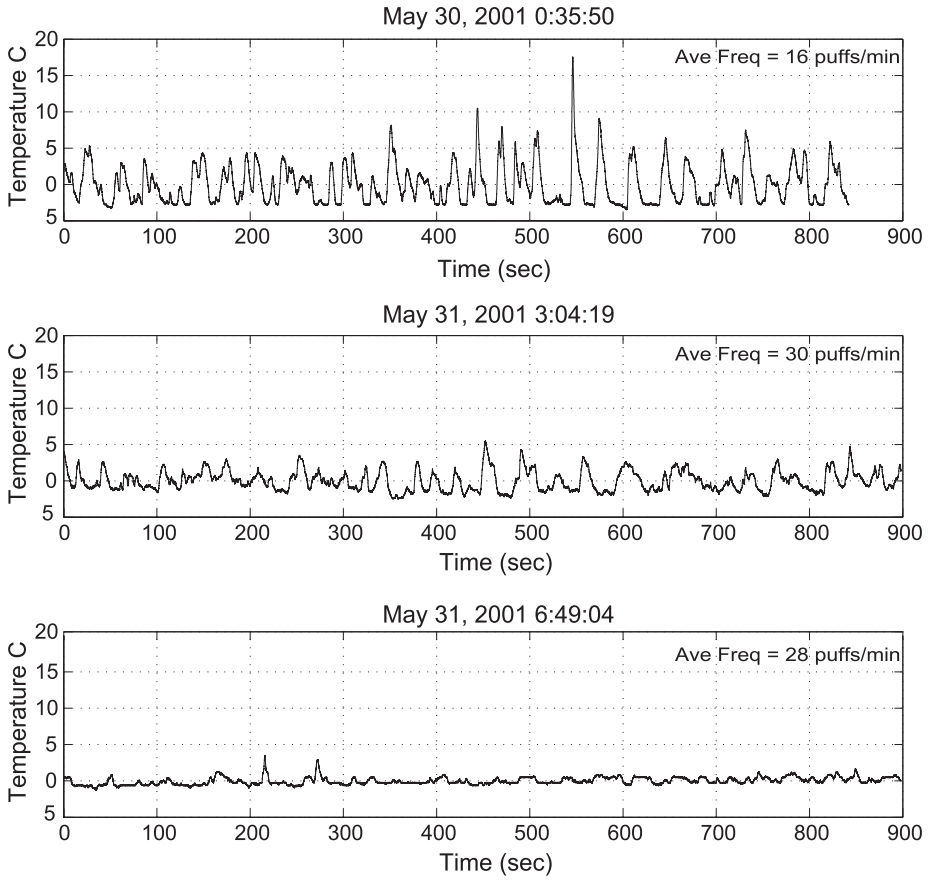

Fig. 4. Three ~15 minute IR-thermometer data sets obtained for SEC puffing. Each spike represents a single gas puff through the IR-thermometer field of view. Note the lack of correlation between the apparent puff amplitude and average puff frequency.

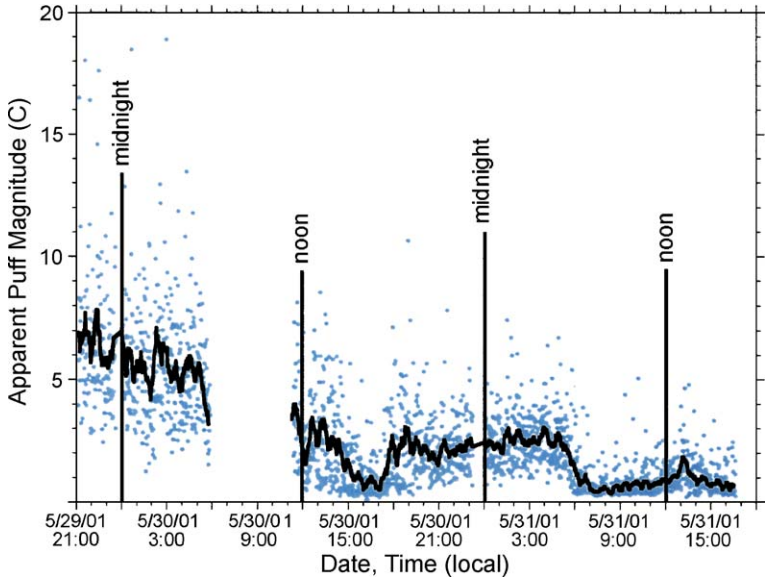

Fig. 5. Plot of apparent puff amplitude versus time, with points representing the maximum puff amplitude per minute. The solid line is a 20-min running mean through the data. Note the apparent diurnal effect, for example, between 18:00 on May 30 and 06:00 on May 31.

diurnal variation affects the apparent thermal amplitude of puffs, our time series is too short to state this definitively. We expect that a longer time series would confirm this to be true. Therefore, our analysis of variation in degassing rate (Section 4.2) incorporates only puff frequency (number of puffs per minute), as given in Fig. 6. This parameter should be unaffected by nonvolcanic, diurnal influences.

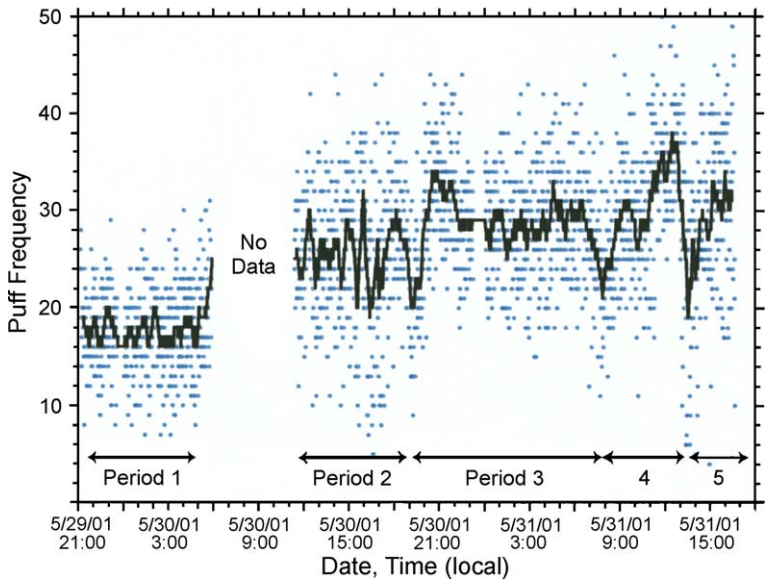

Fig. 6. Plot of puff frequency versus time. Points represent the number of puffs per minute, and the solid line is a 20-min running mean through this data. Five puffing periods are identified on the basis of having a characteristic and relatively persistent puff frequency and/or being bounded by a major decrease in the puffing frequency.

3.3. Effusion rate data and validation

The full long-term effusion rate database is given in Fig. 2. Effusion rate values derived from all methods show relatively good agreement. On May 30, 49 FLIR-derived effusion rate measurements made between 14:45 and 18:38 (local time) give a mean and standard deviation of 2.5 and 0.5 $m^3\ s^{-1}$, with a range of 1.5–4.3 $m^3\ s^{-1}$. These compare with average satellite-based values of 2.4 $m^3\ s^{-1}$ at 00:46 on May 29 and 3.2 and 2.7 $m^3\ s^{-1}$ at 00:36 and 12:12 on May 30, respectively.

In addition, six AVHRR effusion rate values obtained between March 18 and 21 that average 0.24 $m^3\ s^{-1}$ with a range of 0.12–0.61 $m^3\ s^{-1}$ compare with a ground-derived effusion rate of 0.19 $m^3\ s^{-1}$ measured March 20. Another good comparison occurs between March 16 and 22 when three AVHRR-derived effusion rate values averaging 1.45 $m^3\ s^{-1}$ with a range of 1.22–1.89 $m^3\ s^{-1}$ compare with a ground-derived estimate of 1.33 $m^3\ s^{-1}$ on May 17 and 2.45 $m^3\ s^{-1}$ on May 18. Also, ground-based and satellite-derived effusion rate trends during the 2001 flank event are similar (Fig. 2c).

4. Results and discussion

4.1. Long-term effusion rates: oscillations in the erupted flux, January–August 2001

Our AVHRR-derived effusion data for January–August 2001 indicate that the flank eruption of July–August 2001 was preceded by a series of building phases. We identify four pulses that follow an increasing trend (Fig. 2b, Table 1). Volumes shown in Table 1 were obtained by integrating the AVHRR effusion rate values within each pulse through time. This gives a satellite-derived DRE volume for the 2001 flank eruption lava flows of $19.8 \pm 7.7 \times 10^6\ m^3$, which is lower than the ground-based DRE volume of $37.5 \pm 5.5 \times 10^6\ m^3$ for effusive activity. The use of anomalously high or low effusion rate values can introduce significant error into volume estimates derived from satellite-based data (Harris et al., 2000). We therefore emphasize that a time series of effusion rates is more valuable for showing trends in effusion than for obtaining accurate volume estimates, though relative volumes can still be insightful.

4.1.1. Pulses prior to the 2001 flank eruption

Pulse 1 had a duration of ~ 57 days, was characterized by relatively low effusion rates (0.01–1.2 $m^3\ s^{-1}$), and produced ~ $1.3 \times 10^6\ m^3$ of lava, as calculated using satellite thermal data. This pulse coincides with the onset of Strombolian eruptions and variation in effusive activity observed at SEC during January and February 2001. Note that Pulse 1 includes effusion rate spikes on February 7, 16, and 24 (Fig. 2b).

After a decreasing effusion rate trend during February 24 through March 4, we identify a second pulse beginning on March 5. Pulse 2 persisted for ~ 46 days, was also characterized by relatively low effusion rates (0.01–1.1 $m^3\ s^{-1}$), and is volumetrically indistinguishable from Pulse 1. This pulse included two rough phases (March 5–19 and March 20–April 23) and a single effusion rate spike (March 28), subsequent to which our data show declining effusion rates for ~ 25 days until the onset of Pulse 3 (April 24).

Pulse 3 persisted for ~ 55 days through June 18. Due to the cloud-caused scarcity of data from May 4 to 25, it is not possible to determine whether Pulse 3 comprised two spikes occurring on April 27 and May 26, or if their appearance is an artifact introduced by the poor sampling rate during this interval. Pulse 3 had higher effusion rates than the previous two pulses,

Table 1
Effusion rate pulses summary

Pulse no.	Onset date (2001)	End date (2001)	Duration (days)	Peak date	Peak E_r ($m^3\ s^{-1}$)	Volume ($\times 10^6\ m^3$)	Mean E_r ($m^3\ s^{-1}$)	$\sigma\ E_r$ ($m^3\ s^{-1}$)
1	1 January	4 March	57	16 Feb	1.2	1.3	0.4	0.2
2	5 March	21 April	46	28 Mar	1.1	1.3	0.3	0.2
3	24 April	18 June	55	27 May	4.2	6.3	1.4	1.0
4	23 June	16 July	23	28 June	8.8	4.2	1.7	2.0
5	17 July	9 August	23	23 July	22.2	19.8	10.9	6.6

consistent with heightened activity observed at the SEC during this time.

Pulse 4 began June 23, reached a single peak on June 28, and persisted ~ 23 days until the onset of the 2001 flank eruption. This fourth pulse continued the trend of increasing peak and mean effusion rate values (Table 1).

4.1.2. The 2001 flank eruption

The 2001 flank eruption lasted 23 days and involved the largest satellite-derived volume and highest peak and mean effusion rates in 2001 (Table 1). Our time series indicates that the eruption may have comprised two effusive phases that were separated by a reduction in effusive activity (but an increase in explosive activity) during July 24–27 (Fig. 2c). The first episode showed waxing lava effusion rates to a peak of 22.2 ± 9.6 m^3 s^{-1} on July 23, followed by decreasing values to July 27. A second peak of 19.8 ± 6.4 m^3 s^{-1} was reached on July 30, subsequent to which satellite-derived effusion rates steadily declined through to the eruption's conclusion (Fig. 2c).

We note that the lull in effusion during July 24–27 coincides with a change in eruption style at the 2550-m vent. Activity changed from ash-rich subplinian activity to fire fountaining on July 24, and then returned to ash emission on July 27–28. Therefore, the satellite-derived values for lava effusion may be particularly nonrepresentative of the net mass flux (effusive + explosive) during this interval.

4.1.3. Rank-order analysis of the satellite-derived effusion rate time series

We perform a rank-order analysis of the satellite-derived effusion rate data to examine if it would have been possible to identify the change in Etna's eruptive state represented by the 2001 flank eruption. Building on Sornette et al. (1996), Pyle (1998) showed that for volcanic factors such as erupted volume and caldera size, a power-law function defined by rank-order statistics could be derived. Such a plot allows the largest (N) number of events (above a given threshold) to be used to predict the likely magnitude of the next largest occurrence of the same phenomena. Rothery et al. (2001) applied this method to 1.6-μm radiance data from the along track scanning radiometer (ATSR) for vents and flows at Etna. We follow their logic by plotting a time series of thermal data at an active volcanic system. Here, we consider each AVHRR-derived effusion rate value as an event and expect any point that falls off of a linear extension through a given power-law distribution to indicate a change in the state of the system being studied. The AVHRR-derived effusion rate time series defines an exponentially increasing trend prior to the 2001 flank eruption (Fig. 2). Plotting these data in rank order shows a power-law dependency of event frequency on event magnitude, wherein the time series has a high frequency of low effusion rate values and low frequency of higher effusion rate values (Fig. 7).

Fig. 7 shows two rank-order plots of the AVHRR-derived effusion rate time series for 2001. The lower curve is the subset of data from January 1 through July 17 with a trend line plotted through events ranked 4–23. The upper curve includes data from January 1 through August 9, 2001. The top 21 ranked events on this curve occur during the 2001 flank eruption and define a statistically different power-law distribution. The shown trend line is plotted through events ranked 1–17.

Pyle (1998) uses maximum likelihood statistics to show that the function described by N number of events larger than a chosen threshold size, together with the magnitude of the currently ranked number one (largest) event (Z_1^{current}), can be used to predict the most likely magnitude of the next largest event (Z_1^{next}) according to $Z_1^{\text{next}}=[(2\mu+1)/(\mu+1)]^{(1/\mu)}Z_1^{\text{current}}$. In this equation, $\mu=-(1/b)$, b is the exponent of the power-law function, and there is a relative error in μ of $\sim N^{(-1/2)}$. Applying this method to the data ranked 1–20 (i.e. $N=20$) in the January 1 to July 17 data gives the function:

$$y = 7.0377x^{-0.3886} \quad (R^2 = 0.9126)$$

and predicts a next-highest effusion rate of 10.9 ± 0.6 m^3 s^{-1}. Because the three highest ranked data points appear to fall off the trend defined by the data ranked 4–23 (Fig. 7), we also carry out an analysis using $N=20$, but excluding the three highest ranked data points (i.e. using data ranked 4–23). This yields the function:

$$y = 4.8198^{-0.2377} \quad (R^2 = 0.9625)$$

and predicts a next-highest magnitude of 4.2 ± -0.9 m^3 s^{-1}.

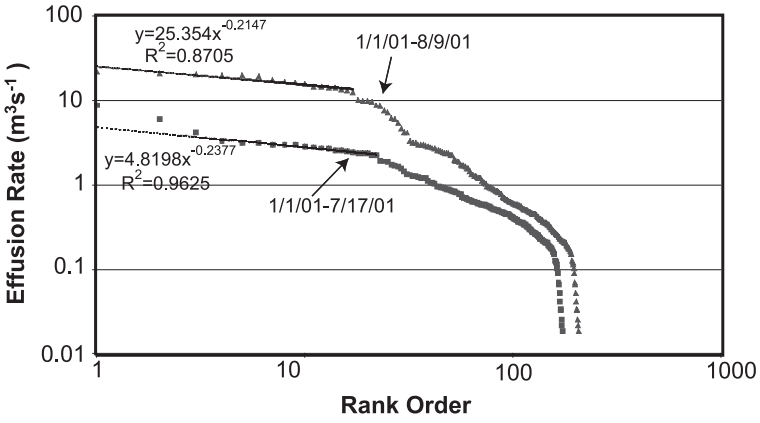

Fig. 7. Log–log rank-order plot of AVHRR-derived effusion rate data. The upper curve includes all data for Jan 1–Aug 9; the lower curve includes only data prior to the 2001 flank eruption (Jan 1–Jul 17). Solid lines are trends through events ranked 1–17 for the upper curve and events ranked 3–23 for the lower curve. Equations shown are the power-law function describing either trend line, with their associated R^2 value. The top 21 ranked effusion rate values on the upper curve are from the 2001 flank eruption, and note that they define a distribution statistically different than that of the lower curve.

Of the 35 AVHRR-derived effusion rates attained during the 2001 flank eruption, the top 17 ranked events fall above the former predicted magnitude of 10.9 $m^3\ s^{-1}$ and the top 27 ranked events fall above the latter value of 4.2 $m^3\ s^{-1}$. Therefore, if we consider the distribution defined by persistent activity at Etna from January 1 to July 17 as background, the statistical distribution of the 2001 flank eruption would, in fact, indicate a change in the volcano's eruptive state. Further, given the sharp increase in AVHRR-derived effusion rate values at the onset of the 2001 flank eruption (i.e. to 12.5 $m^3\ s^{-1}$ on July 18 and 16.8 $m^3\ s^{-1}$ on July 19; see Fig. 2), the change in Etna's activity could have been identified almost immediately using either function given above.

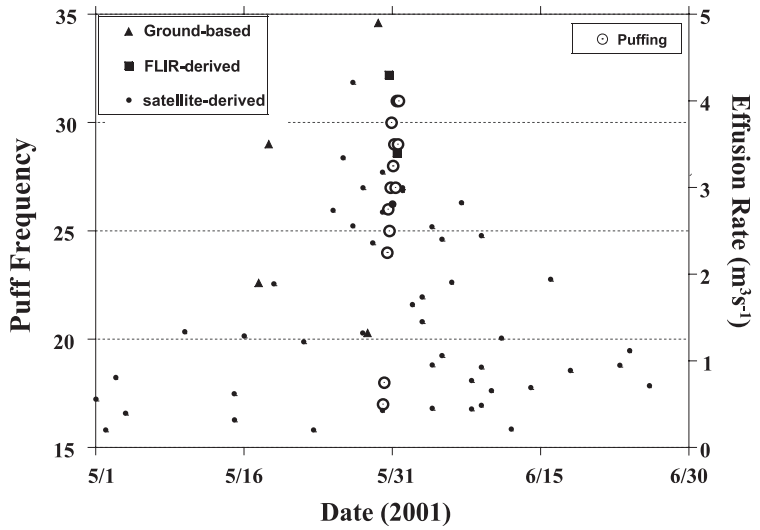

Fig. 8. Plot of puff frequency data for May 29–31 and effusion rate data for May and June 2001. Puffing is plotted as puffs per minute data time-averaged over 3 h at the midpoint time. FLIR-derived effusion rate squares represent the average effusion rate value for May 30 and 31 plotted at the midpoint time for each day.

Petrological data support the change in state represented by the 2001 flank eruption. Two distinct compositions of magma were erupted during this flank event—porphyritic Hawaiite at vents above 2600 m (similar to magma commonly erupted in past centuries and in months preceding the 2001 flank eruption) and unusual porphyritic alkali basalt at vents below 2600 m (Calvari et al., 2001). The addition of a second and unique composition of magma clearly indicates that the volcano had undergone a change in state.

The rank-order analysis yields the unexpected finding that our highest ranked events may define an effusion rate threshold for both Etna's persistent state of activity (particularly if we exclude events ranked 1–3) and the 2001 flank eruption. Notice that both the linear trends in Fig. 7 are relatively flat. Considering the January 1–July 17 subset of data, for events ranked 4–23, $Z_1^{\text{current}} = 3.3\ \text{m}^3\ \text{s}^{-1}$ and, as stated above, the predicted $Z_1^{\text{next}} = 4.2 \pm 0.9\ \text{m}^3\ \text{s}^{-1}$, a difference of only 22%. Considering the upper curve and using $N = 17$ (which includes only data for the 2001 flank eruption) yields the function shown in Fig. 7. For the 2001 flank eruption then, $Z_1^{\text{current}} = 22.2\ \text{m}^3\ \text{s}^{-1}$ and $Z_1^{\text{next}} = 26.0 \pm 0.1\ \text{m}^3\ \text{s}^{-1}$, a difference of

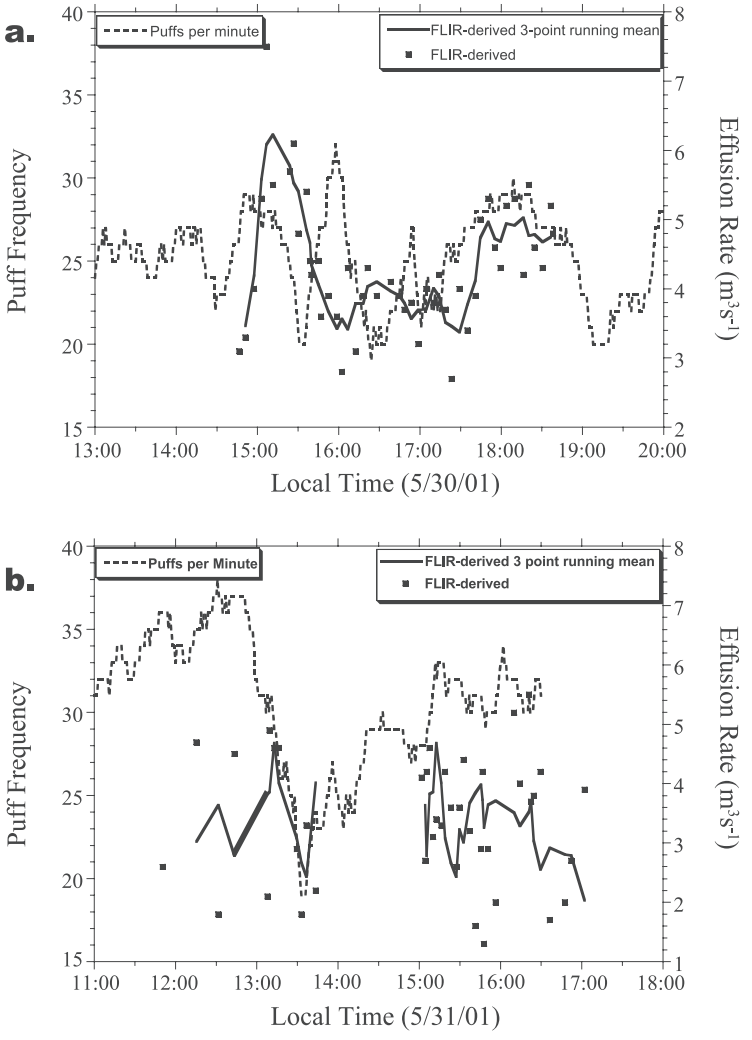

Fig. 9. Plot of puff frequency and FLIR-derived effusion rate data for (a) May 30 (13:00–20:00) and (b) May 31 (11:00–18:00), 2001. Puff frequency data are plotted as puffs per minute time-averaged over 12 min at the midpoint time.

only 15%. Identification of an approximate threshold to effusion rates for Etna's persistent activity would be universally useful in characterizing this state of the volcanic system. It would be worthwhile to conduct a similar analysis using an even longer time series from this common style of activity to check the effusion rate limit of the system we may have identified. Our data indicate a range of $\sim 3-5$ m^3 s^{-1} as the maximum limit for Etna's (non-anomalous) persistent style of activity.

Although episodic flank eruptions at Etna tend to vary in scope and intensity, identification of an approximate maximum effusion rate value for the 2001 flank eruption may provide a starting point for characterizing this state of the system. Our data indicate a potential maximum threshold for flank eruptions at Etna in the range of $25-30$ m^3 s^{-1}. Plotted together in rank order, similar satellite-derived effusion rate data from more flank eruptions would provide insight into whether or not there is consistency in peak effusion rates among multiple events of this nature at Etna.

4.2. Degassing and channel-based effusion rate results: short-term oscillations in the erupted flux, May 29–31, 2001

The puff frequency data presented in Fig. 6 show trends on two time scales: (a) a steady, increasing trend over the measurement period; and (b) hours to minutes oscillation overprinted on the more general trend. The steady increase in puff frequency from May 29 to 31 is broadly consistent with reports of heightened activity over the month of May (as discussed in Section 2). It is also consistent with the satellite-derived peak of Pulse 3 (May 26–June 1) (Fig. 2b) and ground-based high of ~ 5 m^3 s^{-1} for the months of May and June 2001 (Fig. 8).

Our data indicate that a relationship between degassing and effusion rate may exist. For example, satellite-derived and average FLIR-derived effusion rate values both decreased from May 30 to May 31 ($3.2-2.8$ and $4.3-3.4$ m^3 s^{-1}, respectively) (Fig. 8), while puff frequency followed a generally increasing trend. If waning shallow supply of magma drives the decline in effusion, it is possible that the degassing response lags behind the effusion rate response: with a decrease in puff frequency manifesting itself 1–2 days after the initial decrease in effusion rate. A longer set of degassing data and a higher frequency of effusion rate values could help decipher such a relationship more precisely. The detailed channel-based effusion rate and degassing data may indicate a correlation on an even shorter time scale and similar to that found at Stromboli by Ripepe et al. (2002). Fig. 9a shows a surge in effusion rate between $\sim$ 17:30 and 19:00 on May 30 that was coincident with an increase in puff frequency. Also, a decline in puff frequency commencing at $\sim$ 14:50 on May 30 was followed $\sim$ 30 min later by a decline in effusion rate (Fig. 9a). However, the puff frequency peak that occurred at $\sim$ 16:00 on May 30 is not reflected in the effusion rate data, and there is no clear link between puff frequency and effusion rate on May 31 (Fig. 9). Again, a longer time series of data is needed to demonstrate whether or not there is any correlation.

Our working hypothesis is that oscillations in degassing and effusion rate would be related to changes in the supply rate of magma to Etna's shallow

Table 2
Puffing cycles summary

Cycle no.	Onset time (2001)	End time (2001)	Duration (min)	Peak time	Peak frequency (puffs min^{-1})	Mean frequency (puffs min^{-1})	σ frequency (puffs min^{-1})
1	29 May 21:00	30 May 5:54	524	30 May 5:48	31	18	4.3
2	30 May 11:24	30 May 19:28	484	30 May 17:12	44	25	7
3	30 May 19:29	31 May 8:00	751	30 May 22:23	44	29	6
4	31 May 8:01	31 May 13:44	343	31 May 11:48	50	30	7
5	31 May 13:45	31 May 16:40	175	31 May 16:31	49	29	8

(near-vent) conduit system, such that an increase in supply of gas-rich magma would lead to both an amplification in puff frequency and heightened effusion (though not necessarily simultaneously). In an effort to constrain the time scale of potential variations in this supply rate, we grouped the puffing data into five periods (Fig. 6, Table 2) that are either bounded by major decreases in puff frequency (i.e. Period 3) or are characterized by a unique puff frequency (i.e. Period 1). The main periods identified range from 3 to 14 h. Also, 26 oscillations of 19 to 126 min (mean = 82 min, standard deviation = 43 min) can be identified within our data set. These minutes-long oscillations may be related to a third time scale of degassing and possibly supply processes.

5. Conclusions

This study identifies variation in effusion rate at Etna from January through August 2001 on time scales that span minutes to months and variations in degassing that occur over minutes to hours. Furthermore, the time scale of this variation incorporated hours-, days-, and weeks-long oscillations that were overprinted on a consistent ~8-month increase through the 2001 flank eruption.

An important and interesting question to consider is what processes could have driven variation on the multiple time scales we have identified. In a very general sense, two possibilities are: (1) fluctuation in supply rate from the source region; or (2) conduit processes that interfere with an approximately constant supply rate from the source region. Given a constant source supply rate, it is possible that some at-vent variation results from slowed ascent of magma in contact with irregular conduit walls during transport. Another effective process may be convective overturn in shallow portions of the system. In this case, effusion rate surges could be driven by the buoyancy of a relatively gas-rich bleb of magma gathering beneath a relatively degassed cap. If vesiculation continues, the gas-rich body of magma would be expected to push aside (or out) the degassed cap and erupt. If the degassed cap is ejected prior to the gas-rich body, we would expect some lag time between a peak in effusion rate and a peak in puff frequency, such as we observe during Pulse 3.

Following Ripepe et al. (2002), we can also consider a direct link between changing magma supply and changing volatile flux, which should drive consistent variation in the gas puffing frequency and effusion rate. Our data indicate that this may be true, though not conclusively. Longer data sets of these types are needed to identify the presence or absence of a correlation between degassing and mass discharge.

Finally, rank-order analysis of our satellite-derived effusion rate data may reveal a maximum effusion rate threshold in the range of 3–5 $m^3\ s^{-1}$ for Etna's typical persistent activity and 25–30 $m^3\ s^{-1}$ for the 2001 flank eruption. With data from more flank eruptions, the latter result could be expanded to attempt to classify a similar threshold for Etna during episodic flank eruptions. If more data support our findings, it will provoke further investigation into what processes can cause such thresholds to exist.

Acknowledgements

Nicole Lautze thanks the National Weatherservice for funding during this study and the Italian Fulbright Commission for generous backing in Italy in 2000–2001. This study was also supported by the NSF grant EAR-0207734. Authors would like to thank Harold Garbeil for data processing assistance. David Rothery and Dave Pyle provided perceptive and insightful reviews that greatly contributed to the quality of this work. Thanks to Bruce Houghton for a concrete scientific and grammatical review of the paper in a near final state. This paper is HIGP publication number 1263 and SOEST publication number 6095.

References

Allard, P., Carbonnelle, J., Metrich, N., Loyer, H., Zettwoog, P., 1994. Sulphur output and magma degassing budget of Stromboli volcano. Nature, London, 368, 326–330.

Andronico, D., Calvari, S., Lodato, L., in preparation. Eruptive activity at Etna volcano before the 2001 flank eruption.

Calvari, S., INGV-Sezione di Catania Scientific Staff, 2001. Multidisciplinary approach yields insight into Mt. Etna eruption. EOS 82, 653–656.

Calvari, S., Coltelli, M., Neri, M., Pompilio, M., Scribano, V., 1994. The 1991–1993 Etna eruption: chronology and lava flow-field evolution. Acta Vulcanol. 4, 1–14.

Calvari, S., Neri, M., Pinkerton, H., 2003. Effusion rate estimations during the 1999 summit eruption on Mount Etna and growth of two distinct lava flow fields. J. Volcanol. Geotherm. Res. 119 (1–4), 107–123.

Dozier, J., 1981. A method for satellite identification of surface temperature fields of subpixel resolution. Remote Sens. Environ. 11, 221–229.

Dozier, J., 1981. A method for satellite identification of surface temperature fields of subpixel resolution. Remote Sens. Environ. 11, 221–229.

Harris, A.J.L., Rothery, D.A., Carlton, R.W., Langaas, S., Mannstein, H., 1995. Non-zero saturation of AVHRR thermal channels over high temperature targets: evidence from volcano data and a possible explanation. Int. J. Remote Sens. 16, 189–196.

Harris, A.J.L., Blake, S., Rothery, D.A., Stevens, N.F., 1997a. A chronology of the 1991 to 1993 Mount Etna eruption using advanced very high resolution radiometer data: implications for real-time thermal volcano monitoring. J. Geophys. Res. 102, 7985–8003.

Harris, A.J.L., Butterworth, A.L., Carlton, R.W., Downey, I., Miller, P., Navarro, P., Rothery, D.A., 1997b. Low-cost volcano surveillance from space: case studies from Etna, Krafla, Cerro, Fogo, Lascar and Erebus. Bull. Volcanol. 59, 49–64.

Harris, A.J.L., Sherman, S.B., Flynn, L.P., Rothery, D.A., Oppenheimer, C., 1999. Mass flux measurements at active lava lakes: implications for magma recycling. J. Geophys. Res. B: Solid Earth 104 (4), 7117–7136.

Harris, A.J.L., Murray, J.B., Aries, S.E., Davies, M.A., Flynn, L.P., Wooster, M.J., Wright, R., Rothery, D.A., 2000. Effusion rate trends at Etna and Krafla and their implications for eruptive mechanisms. J. Volcanol. Geotherm. Res. 102, 237–270.

Pyle, D.M., 1998. Forecasting sizes and repose times of future extreme volcanic events. Geology 26, 367–370.

Ripepe, M., Harris, A., Carniel, R., 2002. Thermal, seismic and infrasonic evidences of variable degassing rates at Stromboli Volcano. J. Volcanol. Geotherm. Res. 118, 285–297.

Rothery, D.A., Francis, P.W., Wood, C.A., 1988. Volcano monitoring using short wavelength infrared data from satellites. J. Geophys. Res. 93, 7993–8008.

Rothery, D.A., Coltelli, M., Pirie, D., Wooster, M.J., Wright, R., 2001. Documenting surface magmatic activity at Mount Etna using ASTR remote sensing. Bull. Volcanol. 63, 387–397.

Sornette, D., Knopoff, L., Kagan, Y.Y., Vanneste, C., 1996. Rank-ordering statistics of extreme events; application to the distribution of large earthquakes. J. Geophys. Res. 101, 13,883–13,893.

Swanson, D.A., Duffield, W.A., Jackson, D.B., Peterson, D.W., 1979. Chronological narrative of the 1969–71 Mauna Ulu eruption of Kilauea Volcano, Hawaii. US Geol. Surv. Prof. Pap. 1056, 55 pp.

Tilling, R.I., Christiansen, R.L., Duffield, W.A., Endo, E.T., Holcomb, R.T., Koyanagi, R.Y., Peterson, D.W., Unger, J.D., 1987. The 1972–1974 Mauna Ulu eruption, Kilauea Volcano; an example of quasi-steady-state magma transfer Volcanism in Hawaii. US Geol. Surv. Prof. Pap. 1350, 405–409.

Wadge, G., 1981. The variation of magma discharge during basaltic eruptions. J. Volcanol. Geotherm. Res. 11, 139–168.

Wright, R., Blake, S., Harris, A.J.L., Rothery, D.A., 2001. A simple explanation for the space-based calculation of lava eruption rates. Earth Planet. Sci. Lett. 192, 223–233.